








Article

Carbon Nanomaterials from Polyolefin Waste: Effective Catalysts for Quinoline Degradation through Catalytic Wet Peroxide Oxidation

Fernanda F. Roman ^{1,2,3,4,*} , Larissa De Grande Piccinin ^{1,2,5}, Adriano Santos Silva ^{1,2,3,4} , Jose L. Diaz de Tuesta ⁶, Isabella V. K. Freitas ^{1,2,7}, Admilson Vieira ⁵ , Giane Gonçalves Lenzi ⁷ , Adrián Manuel Tavares Silva ^{3,4} , Joaquim Luís Faria ^{3,4}  and Helder Teixeira Gomes ^{1,2,*} 

- ¹ Centro de Investigação de Montanha (CIMO), Instituto Politécnico de Bragança, Campus de Santa Apolónia, 5300-253 Bragança, Portugal; isaveroniica@hotmail.com (I.V.K.F.)
- ² Laboratório Associado para a Sustentabilidade e Tecnologia em Regiões de Montanha (SusTEC), Instituto Politécnico de Bragança, Campus de Santa Apolónia, 5300-253 Bragança, Portugal
- ³ LSRE-LCM—Laboratory of Separation and Reaction Engineering—Laboratory of Catalysis and Materials, Faculdade de Engenharia, Universidade do Porto, Rua Dr. Roberto Frias, 4200-465 Porto, Portugal; jlfaria@fe.up.pt (J.L.F.)
- ⁴ ALiCE—Associate Laboratory in Chemical Engineering, Faculdade de Engenharia, Universidade do Porto, Rua Dr. Roberto Frias, 4200-465 Porto, Portugal
- ⁵ Universidade Tecnológica Federal do Paraná, Campus Londrina, Londrina 86036-370, Brazil; lopesvieira@utfpr.edu.br
- ⁶ Chemical and Environmental Engineering Group, ESCET, Rey Juan Carlos University, Tulipán s/n, 28933 Móstoles, Spain; joseluis.diaz@urjc.es
- ⁷ Universidade Tecnológica Federal do Paraná, Campus Ponta Grossa, Ponta Grossa 84017-220, Brazil; gianeg@utfpr.edu.br
- * Correspondence: roman@ipb.pt (F.F.R.); htgomes@ipb.pt (H.T.G.)



Citation: Roman, F.F.; De Grande Piccinin, L.; Santos Silva, A.; Diaz de Tuesta, J.L.; Freitas, I.V.K.; Vieira, A.; Gonçalves Lenzi, G.; Manuel Tavares Silva, A.; Faria, J.L.; Gomes, H.T. Carbon Nanomaterials from Polyolefin Waste: Effective Catalysts for Quinoline Degradation through Catalytic Wet Peroxide Oxidation. *Catalysts* **2023**, *13*, 1259. <https://doi.org/10.3390/catal13091259>

Academic Editor: Mingjun Jia

Received: 4 August 2023

Revised: 25 August 2023

Accepted: 28 August 2023

Published: 30 August 2023



Copyright: © 2023 by the authors. Licensee MDPI, Basel, Switzerland. This article is an open access article distributed under the terms and conditions of the Creative Commons Attribution (CC BY) license (<https://creativecommons.org/licenses/by/4.0/>).

Abstract: Quinoline (QN) is highly toxic and carcinogenic and has been detected in soil, groundwater, and biological tissues. Advanced oxidation processes (AOPs) have shown promise to address its degradation in wastewater treatment, with catalytic wet peroxide oxidation (CWPO) being highlighted due to its cost-effectiveness and mild operation. However, developing active and inexpensive catalysts is crucial for CWPO's effectiveness. Another pressing issue is the accumulation of mixed, dirty plastic solid waste (PSW), particularly polyolefins used in packaging. Although recycling rates have increased, much plastic packaging remains in landfills. However, polyolefins can be converted into carbon-based nanostructured materials (CNMs), such as carbon nanotubes (CNTs), through chemical vapor deposition (CVD) using PSW as a carbon precursor. While many studies focus on CNT preparation, their application is often overlooked. In this context, this work proposes the preparation of CNMs, particularly CNTs, through CVD using a single-stage pyrolysis reactor. Polyolefins (LDPE, HDPE, and PP), both individually and in a mixture simulating PSW, were used as carbon sources. Given a sufficiently high temperature, the desired CNT architecture was successfully synthesized regardless of the starting polymer. These CNMs were then tested as catalysts for CWPO in simulated wastewater containing QN. The results showed a rapid degradation of QN (30–120 min) and high removals of total organic carbon (TOC) and aromatic compounds (75% and >90%, respectively), demonstrating the applicability of PSW-derived CNTs in the CWPO process for QN abatement.

Keywords: plastic solid waste; heterogeneous fenton; advanced oxidation processes

1. Introduction

Quinoline (QN) is a nitrogenated heterocyclic aromatic compound widely used in various industries, such as pharmaceutical and chemical industries [1]. It is ubiquitous to crude oils, and, thus, it is commonly found in wastewater from petrochemical facilities [1], with reported concentrations varying from 7.2 mg L^{−1} [2] to as high as 57 mg L^{−1} [3]

for coking wastewater and 82 mg L^{-1} for a sewage sample [4]. QN is highly toxic and carcinogenic with high mobility, resulting in its detection in soil, groundwater, and even biological tissues [5]. Furthermore, QN is not easily biodegraded, requiring alternative technologies for its degradation. Advanced oxidation processes (AOPs) have shown promising results for removing QN [6–9]. Among AOPs, catalytic wet peroxide oxidation (CWPO) can be highlighted due to its low cost and mild operation [10]. CWPO relies on the formation of highly oxidizing hydroxyl radicals from hydrogen peroxide through the action of a suitable catalyst [11]. CWPO has been tested for the oxidation of several organic compounds with distinct catalysts [12–16], showing effective results in the degradation of organic pollutants. Nevertheless, developing active and inexpensive catalysts is still a key step for CWPO implementation.

Another issue currently faced is the accumulation of mixed dirty plastic solid waste (PSW) since recycling this plastic fraction is challenging. According to forecasts on the introduction of microplastics into aquatic and terrestrial ecosystems [17], innovative approaches to recycling these wastes are needed to significantly reduce the amount of microplastics entering those environments [17]. Polyolefins are frequently found as constituents in dirty PSW, considering they are often employed for packaging [18]. Even though recycling rates for packaging plastics have increased, data from 2020 indicate that around 23% of plastic packaging is still sent to landfills [18]. However, since polyolefins are primarily made of carbon (i.e., low- and high-density polyethylene, LDPE and HDPE, respectively, and polypropylene, PP, are made up of 85.6% of carbon), they can be converted into carbon-based nanostructured materials (CNMs), such as carbon nanotubes (CNTs) [19–25], graphene [26], or others [27]. Specifically, CNTs can be produced via chemical vapor deposition (CVD) using the solid PSW as a carbon precursor [28]. During CVD, the solid PSW fraction is cracked into several gaseous products, and those carbon-rich gases are then deposited into a suitable metal substrate for the growth of the nanostructures [28]. There has been a great development in the obtention of CNTs from residual precursors [29,30], including PSW [27,31]. Nevertheless, most papers focus only on the preparation of the CNTs. There is a lack in the literature regarding the applicability of such types of CNMs [19].

Thus, this work aims at evaluating the use of polyolefins as precursors for obtaining active catalysts for CWPO purposes. Therefore, it proposes the preparation of CNMs, specially CNTs, via CVD using a single-stage pyrolysis reactor. Polyolefins (LDPE, HDPE, and PP), individually and in a mixture, were considered carbon sources for the process, simulating PSW. The desired CNT architecture was successfully synthesized regardless of the starting polymer, given that the temperature was high enough. The obtained CNMs were then tested as catalysts for the CWPO of simulated wastewater containing QN. As far as we know, no other works report the use of waste-based CNTs for QN degradation via AOPs.

2. Results and Discussion

2.1. Materials Synthesis and Characterization

2.1.1. Catalyst for Chemical Vapor Deposition

The X-ray diffraction (XRD) of the CVD catalyst used to grow the CNT structures is shown in Figure 1a. The results were analyzed with the aid of the software X'Pert HighScore Plus (v 4.5) loaded with Crystallography Open Database (COD) cards. The qualitative analysis revealed that samples comprise alumina, hematite, and magnetite, according to cards 96-152-8248, 96-900-9783, and 96-900-6248 from COD, as shown in Figure S1. The semi-quantitative analysis, also obtained with the aid of X'Pert HighScore Plus, revealed that the metal substrate has 76% alumina (Al_2O_3), 22% hematite (Fe_2O_3), and 1% magnetite (Fe_3O_4). The qualitative and quantitative analysis result demonstrates that the material is composed of mixed iron oxide phases supported on alumina, and the content of iron oxide is similar to the intended content of 20%. A similar metal substrate composition was found in previous studies using a similar procedure to prepare the metal substrate for CNTs growth via CVD [12]. The content of Fe, as obtained via atomic absorption, was

determined to be 15 wt.%, corresponding to approximately 21 wt.% of hematite, close to the values observed via XRD.

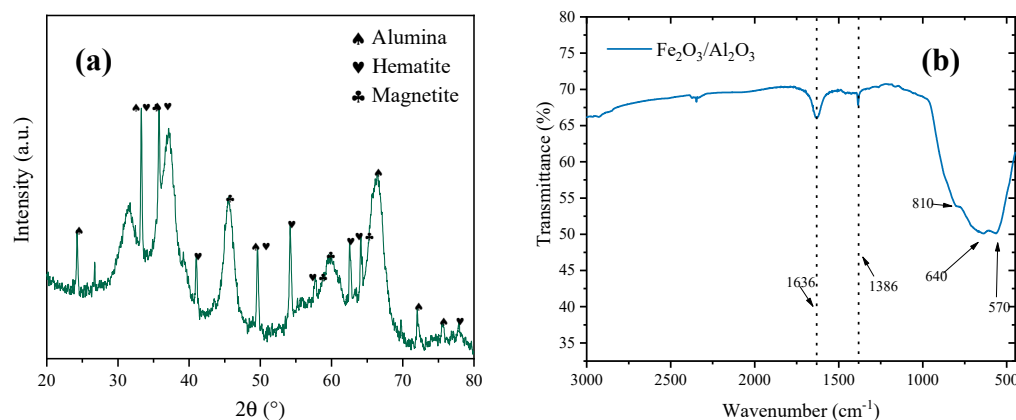


Figure 1. (a) XRD and (b) FTIR of the metal catalyst used in CVD.

FTIR of the metal substrate $\text{Fe}_2\text{O}_3/\text{Al}_2\text{O}_3$ is displayed in Figure 1b. Bands related to adsorbed water were identified ($-\text{OH}$ stretching vibration at 3450 and 1636 cm^{-1}). The bands at 640 and 570 cm^{-1} were ascribed to the vibration of $\text{Fe}-\text{O}$ bonds related to iron oxide phases [32] and the band at 810 cm^{-1} to $\text{Al}-\text{O}$ stretch from alumina [33].

2.1.2. Carbon Nanotubes

The morphology of the prepared samples was observed via TEM, and the images are shown in Figure 2. As observed, the synthesis carried out at 600 $^{\circ}\text{C}$ did not allow for obtaining filamentous structures as expected. However, a crystalline carbon phase can be observed encapsulating an iron particle on the left side of the figure (Figure 2a). The sample also presents amorphous structures (Figure S2). Similar observations have been reported, with CNTs being obtained only at $T > 680$ $^{\circ}\text{C}$ [34]. However, all samples obtained at 800 $^{\circ}\text{C}$ resulted in filamentous structures with hollow cavities, evidencing the shape of CNTs obtained using $\text{Fe}_2\text{O}_3/\text{Al}_2\text{O}_3$ for any polyolefin feedstock or even using a mixture of them. The mechanism of CNTs formation depends on a series of factors, and two main steps are generally assumed: (i) the adsorption of the carbon-rich gas in the catalyst and (ii) a competition between the diffusion of the carbon to the edge of the catalyst particle to form the hollow CNT or the accumulation of carbon on the catalyst to form amorphous carbon [35]. The diffusion or not of the carbon will depend on the catalytic particles [36] and the temperature of the process [35]. For Fe -based catalysts, it has been observed that lower temperatures (below 700 $^{\circ}\text{C}$) favor the formation of amorphous carbon on the catalyst particle, hindering the growth of CNTs, whereas temperatures in the range of 750 – 800 $^{\circ}\text{C}$ favor diffusion and CNT growth [35].

All CNT samples have a similar configuration, with straight walls and a similar number of walls (25–27). The outer diameter was also similar for all samples, with average diameters of 32 ± 5 , 29 ± 1 , 26 ± 1 , and 33 ± 3 nm for CNT-LDPE-800, CNT-HDPE-800, CNT-PP-800, and CNT-MIX-800, respectively, evidencing no significant difference among CNTs obtained from different carbon feedstocks, indicating that the morphology of the CNTs is not affected for the carbon precursors used in this work. For CNM-LDPE-600, the average particle size could not be determined due to its more amorphous structure. In sample CNT-MIX-800, an encapsulated metal particle can be observed in the upper right corner (Figure 2e) because iron nanoparticles are taken from alumina support during CNTs synthesis, as is well known in the mechanism of CNTs growth [12]. As metallic particles are inside the nanotubes, purification methods are not able to remove them without destroying the whole structure. Nevertheless, the metallic phases can work as active phases for the catalytic application of the CNTs and are typically protected against deactivation mechanisms, such as leaching [19]. The outer diameters reported here are similar to

previously reported values for polymer-derived CNTs: 37–44 nm for polyolefin-derived CNTs [12], 4–63 nm for LDPE-derived CNTs [19], 1–40 nm for a mixture of polyolefins [37], and 5–25 nm for polyolefins and polystyrene-derived CNTs [38]. SEM micrographs of the CNT-C sample can be found elsewhere [39].

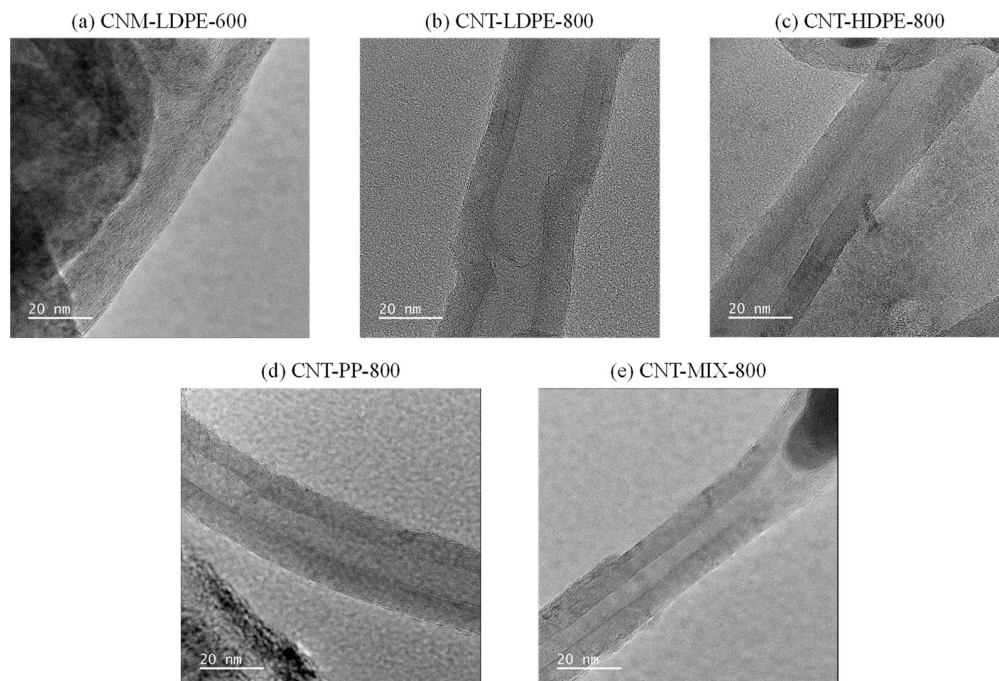


Figure 2. TEM images of (a) CNM-LDPE-600, (b) CNT-LDPE-800, (c) CNT-HDPE-800, (d) CNT-PP-800, and (e) CNT-MIX-800.

The yields of as-synthesized materials are reported in Figure S3. The lowest yield was obtained for the sample synthesized at 600 °C (20 wt.%), which does not present nanotubes. The CNTs synthesized at 800 °C displayed a yield ranging from 26–32 wt.%, depending on the carbon source. The increase in carbonaceous material yields when the temperature increases has been previously reported [40–43]. The highest yield was obtained from the cracking of LDPE at 800 °C (32 wt.%), likely because of its higher selectivity towards small-chain hydrocarbons (i.e., gaseous products) instead of hydrocarbons with longer chains that mostly result in liquid products during pyrolysis. Previous studies in the catalytic cracking of polyolefins for the production of liquid fuels have found that LDPE resulted in the highest selectivity towards C1–C4 hydrocarbons compared to HDPE [44] and compared to PP [45], especially towards methane, ethane, and ethylene gases [46]. The mass loss of CNTs from acid washing is also reported in Figure S3. As observed, a mass loss in the range of 45–60 wt.% was obtained among all samples due to removing inorganic matter (catalysts of CVD). The highest weight losses (55–60 wt.%) were observed for CNTs synthesized at 800 °C versus 45 wt.% for the amorphous sample at 600 °C.

Figure 3 displays the results obtained for the TGA of the purified carbonaceous samples in the air atmosphere. The thermogravimetric profile also changes greatly depending on the temperature of the CVD process. For CNM-LDPE-600 (Figure 3a), two distinct regions of mass loss are evident: one centered at 410 °C and the main one centered at 550 °C. The region with the lower temperature, corresponding to approximately 5 wt.% of CNM-LDPE-600, is mostly related to the deposition of amorphous carbon on the catalyst, corroborating the results observed via TEM. In contrast, the region with higher temperatures is related to the deposition of highly graphitic carbon structures, such as graphene layers, which was also observed on TEM images. However, the CNTs synthesized at 800 °C do not demonstrate the presence of amorphous carbonaceous structures, as the mass loss is mostly centered between 585 and 600 °C (Figure 3b–d), which also indicates that the use of different polyolefins does

not seem to impact the center of mass loss. Other authors have also observed that increasing the temperature increases the degree of graphitization of the CNTs [42,47]. Similar profiles for TGA/DTG curves have been previously reported [12,13]. Furthermore, as oxidative conditions were used, the mass at the end of the process is typically associated with the inorganic matter (ashes) of the materials. In this case, this quantity may be ascribed to the encapsulated iron nanoparticles along carbon structures, which were resistant to the purification conducted via acid attack. As can be seen, the ashes of the carbonaceous materials are within the same range (18–20 wt.%) for the materials synthesized at the same temperature with single polymers (CNT-LDPE-800, CNT-HDPE-800, and CNT-PP-800). CNT-MIX-800 resulted in 25 wt.% of ashes and CNM-LDPE-600 in 28 wt.%.

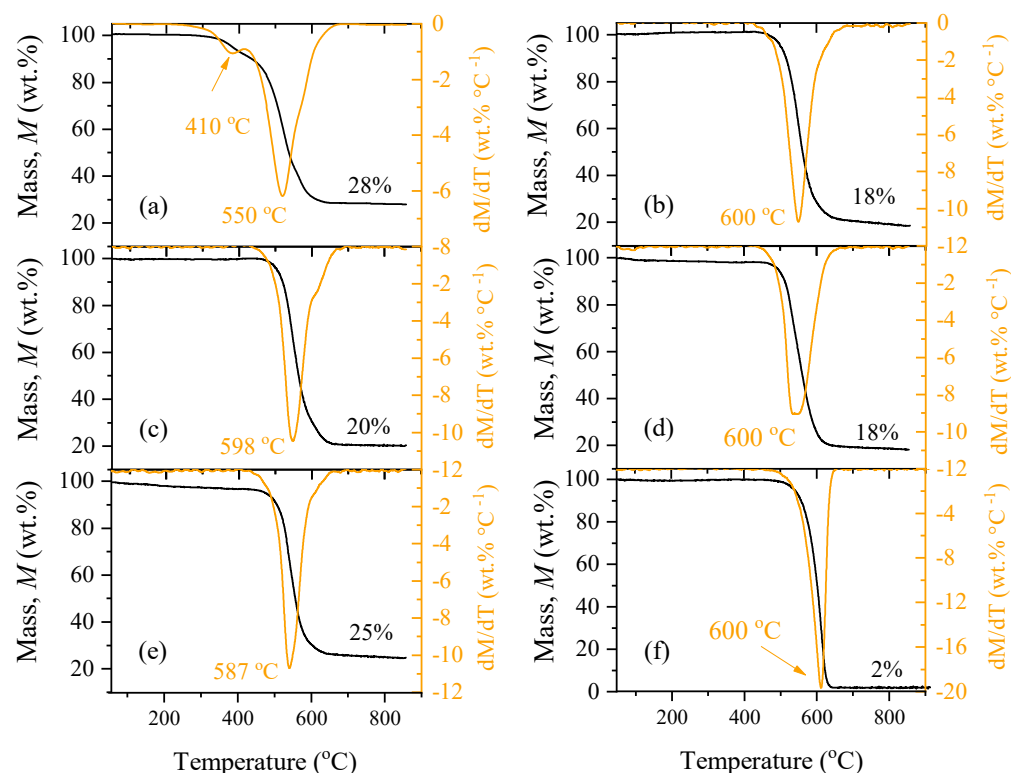


Figure 3. TGA analysis of (a) CNM-LDPE-600, (b) CNT-LDPE-800, (c) CNT-HDPE-800, (d) CNT-PP-800, (e) CNT-MIX-800, and (f) CNT-C.

In this work, commercial CNTs (CNT-C) have also been characterized (Figure 3f) and tested to compare them with those findings obtained for CNTs prepared from plastics. The commercial sample shows a mass loss centered at 600 °C, which is similar to those observed for CNTs prepared from polyolefins. However, ash content resulted in 2 wt.%, which is likely because the mechanism growth, operating conditions (carbon precursor, temperature, flow and pressure), and purification methods are different and are focused on obtaining a highly purified CNT, avoiding the feasible encapsulation of metals inside CNT structures for catalytic proposals.

The textural properties are reported in Table 1, and the adsorption–desorption profiles can be found in Figure S4. The BET surface area (S_{BET}) has varied from 159 to 242 m² g^{−1} for the CNT sample synthesized from polymeric materials, whereas the commercial sample has a surface area of 254 m² g^{−1}. The temperature of the synthesis seems to influence the surface area, as CNM-LDPE-600 (159 m² g^{−1}) resulted in a significantly lower surface area than CNT-LDPE-800 (235 m² g^{−1}) and all other CNTs synthesized at 800 °C (≥ 189 m² g^{−1}). The lowest surface area for CNM-LDPE-600 agrees with TEM observations, since no nanotubes were formed, only graphene layers around the catalyst particles. The total volume of pores followed a similar pattern, varying from 406 to 595 mm³ g^{−1} (and 690 mm³ g^{−1}

for CNT-C), with CNM-LDPE-600 ($406 \text{ mm}^3 \text{ g}^{-1}$) resulting in the lowest volume of pores compared to CNT-LDPE-800 ($594 \text{ mm}^3 \text{ g}^{-1}$). Similar results were previously reported for CNT samples [13].

Table 1. Textural properties of the CNT samples and the CVD metal substrate.

Material	S_{BET} ($\text{m}^2 \text{ g}^{-1}$)	V_{total} ($\text{mm}^3 \text{ g}^{-1}$)
CNM-LDPE-600	159	406
CNT-LDPE-800	235	594
CNT-HDPE-800	189	456
CNT-PP-800	242	595
CNT-MIX-800	194	496
CNT-C	254	690
$\text{Fe}_2\text{O}_3/\text{Al}_2\text{O}_3$	98	273
Al_2O_3	185	437

The infrared spectrum of the materials is reported in Figure 4. A band located at 1582 cm^{-1} was identified for all samples, which was ascribed to the stretching vibration of C=C bonds of either CNT structures or graphene layers [48]. For CNM-LDPE-600, two other bands were identified at 2920 and 2853 cm^{-1} , which were ascribed to the stretching vibration of C-H bonds in $-\text{CH}_2$ groups [48], which could be attributed to defects in crystalline structures [49]. The band at 1386 cm^{-1} is ascribed to O-H bending resulting from adsorbed water.

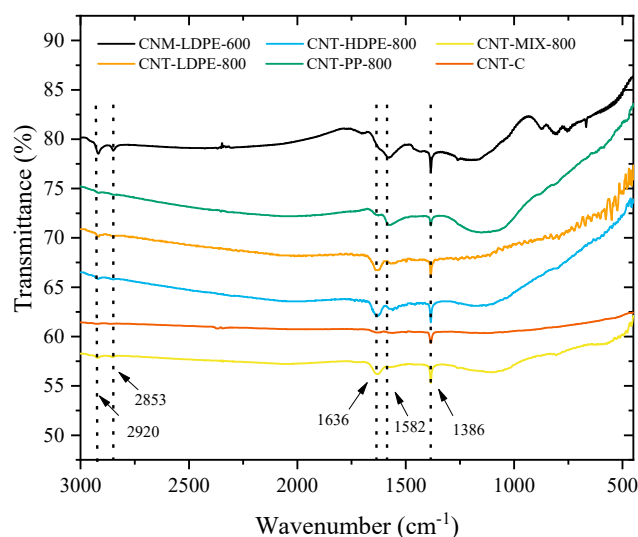


Figure 4. FTIR analysis of the samples.

The elemental analysis of the samples is described in Table 2. As expected, CNM-LDPE-600 resulted in the lowest carbon content among the samples and the highest incorporation of hydrogen and oxygen, likely due to the acid treatment. The higher incorporation of oxygen and hydrogen by CNM-LDPE-600 can be ascribed to its less crystalline structure compared to the other samples: amorphous carbon phases, which were observed for CNM-LDPE-600 and not for the remaining CNTs, can be more easily oxidized during acid treatment [50]. Among the samples synthesized at 800°C , there is also a tendency: LDPE results in the highest C content, followed by HDPE, PP, and, lastly, the mixture of polymers (MIX).

Table 2. Elemental composition of the CNT samples.

Material	C (wt.%)	H (wt.%)	N (wt.%)	S (wt.%)	O (wt.%)	Remaining (wt.%)	Fe (wt.%)
CNM-LDPE-600	70.6 ± 2.1	1.77 ± <0.01	0.07 ± <0.01	0.12 ± <0.01	4.50 ± 0.01	23.0	9.7 ± 0.0
CNT-LDPE-800	86.2 ± 1.1	0.32 ± 0.04	0.10 ± 0.01	0.08 ± 0.01	0.88 ± 0.07	12.5	11.3 ± 0.2
CNT-HDPE-800	85.3 ± 0.5	0.27 ± 0.02	0.09 ± <0.01	0.14 ± 0.01	0.83 ± 0.03	13.4	14.0 ± 0.7
CNT-PP-800	84.1 ± 2.6	0.41 ± 0.01	0.11 ± <0.01	0.18 ± 0.03	1.18 ± 0.01	15.9	11.9 ± 0.7
CNT-MIX-800	80.5 ± 3.6	0.34 ± 0.03	0.00 ± <0.01	0.36 ± 0.09	1.83 ± <0.01	17.0	14.9 ± 0.1

Similarly, CNT-MIX-800 resulted in higher incorporations of O and H compared to the CNT samples obtained from single polymers. The results agree with TGA observations: CNT-MIX-800 resulted in a slightly lower oxidation temperature (587 °C) compared to the remaining samples (598–600 °C), which could be related to the introduction of those oxygenated surface groups [51]. It should be noted that the remaining weight displayed in Table 2 does not match the ashes content calculated via TGA, which can be ascribed to a total or partial oxidation of the metallic particles during TGA in the air atmosphere. Previous works have demonstrated that iron oxides reduce to a cementite phase (Fe-C) during CVD of polymers [12] or even to Fe⁰ [52]. In fact, the reduction of iron at high temperatures (>230 °C) in the presence of carbon is a well-known process [53], so iron can be reduced during the process under study in this work. Upon TGA in air, a mass increase of up to 143% can be expected for the oxidation of Fe⁰ to Fe₂O₃ [54] for temperatures above 600 °C or up to 128% for the oxidation of Fe⁰ to FeO. Previous works have also reported a mass increase of 132% on average for Fe⁰ starting at 450 °C up to 585 °C [55]. The content of Fe is also reported in Table 2. As observed, the remaining content is very close to the iron content, further reinforcing the possibility of partial oxidation during TGA analysis. The highest content of iron was found for CNT-MIX-800 (14.9 wt.%), whereas CNM-LDPE-600 resulted in the lowest (9.7 wt.%), indicating that CNT-MIX-800 resulted in more encapsulation of metallic particles during CVD, whereas CNM-LDPE-600 did not, allowing for the metallic content to be more easily removed during acid treatment. The remaining samples resulted in iron content in the range of 11–14 wt.%.

2.2. Catalytic Wet Peroxide Oxidation of Quinoline

The results for the CWPO of QN are displayed in Figure 5. As seen, the degradation of QN in the presence of the CNTs synthesized in this work is very fast, resulting in over 90% of QN abatement in 30–60 min of reaction time, depending on the CNTs (Figure 5a). In comparison, the non-catalytic run (N.C.) required over 240 min for a similar result, and the commercial CNT sample (CNT-C) required around 120 min. In fact, in less than 30 min of reaction, most of the CNTs synthesized in this work resulted in over 80% of QN abatement, except for CNM-LDPE-600, with 50% degradation. In the same timeframe, the N.C. run resulted in less than 1% removal and the commercial CNT sample (CNT-C) in about 60% abatement, indicating that the CNTs synthesized in this work are more active than the commercial sample. The catalyst for CVD (Fe₂O₃/Al₂O₃) also resulted in a fast abatement of QN; however, it could not completely oxidize the pollutant, ending the reaction with around 5% of the initial concentration of QN still present. There seems to be a synergistic effect for CNTs bearing metallic phases compared to pure Fe₂O₃/Al₂O₃, and this enhanced effect when carbon layers are present has been previously reported for the CWPO of a range of pollutants [56–58]. The synergistic effect between metal phases and carbon layers results from the contribution of both parts to the electron transfer due to their electron-donor ability [58].

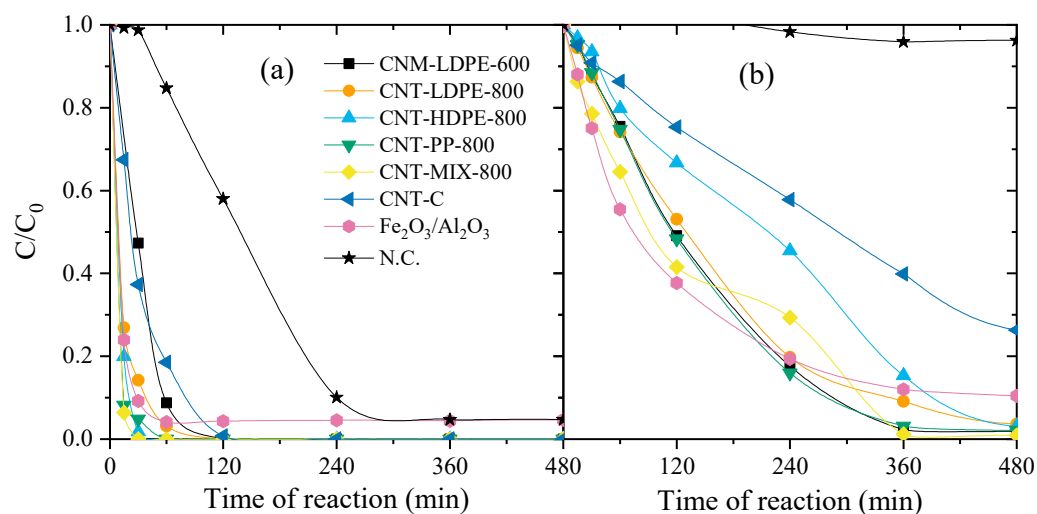


Figure 5. Normalized concentration of (a) QN and (b) H_2O_2 during CWPO runs in the presence of the catalysts. Conditions: $\text{pH}_0 = 3.0$, $[\text{QN}]_0 = 100 \text{ mg L}^{-1}$, $c_{\text{cat}} = 2.5 \text{ g L}^{-1}$, $T = 80^\circ \text{C}$, and $[\text{H}_2\text{O}_2]_0 = 6.2 \text{ g L}^{-1}$.

For the N.C. run, detecting three oxidized compounds in HPLC was also possible (detected in each oxidation experiment at the retention times of 1.86, 2.15, and 3.89 min, for compounds #1, #2, and #3, respectively, at the analytical conditions used for QN), although they were not identified (Figure S5a). All those compounds show a maximum concentration between 120 and 360 min, meaning that the reaction intermediates are also oxidized. Two intermediates (#1 and #3) persisted until the end of the experiment, whereas intermediate #2 was fully degraded in 6 h of reaction. The literature reports that a series of reaction products can arise from QN oxidation via AOPs. The reaction products seem to depend on the radical, with sites with a higher electron density being mainly attacked by the electrophilic HO^\bullet [8]; thus, in this system, QN is expected to be initially attacked in the benzene ring, leading to 8-hydroxyquinoline [5,8] further being oxidized into other intermediates still containing the aromatic ring [8,59]. By the end of the reaction, low-molecular-weight carboxylic acids, such as oxalic, acetic, and formic acids [59,60], as well as propionic and fumaric acids [60], are mostly identified and can be further mineralized. In catalyzed reactions, no intermediates were detected, probably due to their fast formation and subsequent degradation, leading to, most likely, low-molecular-weight carboxylic acids, water, and carbon dioxide.

The behavior towards H_2O_2 consumption varied significantly among the CNTs (Figure 5b). The activity towards H_2O_2 decomposition follows the order $\text{Fe}_2\text{O}_3/\text{Al}_2\text{O}_3 > \text{CNT-MIX-800} > \text{CNT-PP-800} \sim \text{CNM-LDPE-600} \sim \text{CNT-LDPE-800} > \text{CNT-HDPE-800} > \text{CNT-C}$ (data from 1 h of reaction), and complete decomposition of the oxidant was observed in 2–8 h, depending on the catalyst, except for CNT-C and the CVD substrate ($\text{Fe}_2\text{O}_3/\text{Al}_2\text{O}_3$). In the same timeframe, N.C. resulted in less than 10% decomposition of H_2O_2 . The distinct behavior in the decomposition of H_2O_2 vs. abatement of QN can be explained by the fact that the chosen H_2O_2 concentration surpasses the stoichiometric concentration needed for QN mineralization; thus, not all oxidant needs to be consumed to ensure QN degradation. Furthermore, we can observe that the fastest consumption of H_2O_2 was obtained in the presence of $\text{Fe}_2\text{O}_3/\text{Al}_2\text{O}_3$, indicating that the metallic particles may influence the rate of H_2O_2 decomposition. Nevertheless, the rate of decomposition of the oxidant is not the only factor needed for ensuring pollutant degradation, and often the presence of carbon results in a synergistic effect [61]: in fact, in this work, most CNT particles allowed complete H_2O_2 decomposition in 360–480 min of reaction, whereas $\text{Fe}_2\text{O}_3/\text{Al}_2\text{O}_3$ required over 8 h of reaction for 100% decomposition.

The TOC abatement after 24 h of reaction is seen in Figure 6. As observed, the mineralization of QN ranged between 19% for the N.C. and 75% in the presence of CNT-MIX-800, followed closely by CNT-LDPE-800 (73%). The other catalysts resulted in abatements in

the range of 33–63%, with CNM-LDPE-600 and CNT-C being highlighted for their low removals. The pH at the end of the reaction (Figure S5b) was below the initial pH for all runs except for the run conducted in the presence of CNM-LDPE-600 and with $\text{Fe}_2\text{O}_3/\text{Al}_2\text{O}_3$. Compared to the initial value, the pH reduction may be ascribed to the formation of low-molecular-weight carboxylic acids not detected via HPLC. This conclusion is also reinforced when analyzing the concentration of other aromatic compounds (ARMs) in the reaction medium by the end of the reaction: over 70% of the ARMs were removed in the presence of CNTs (Figure S5c), whereas in the presence of $\text{Fe}_2\text{O}_3/\text{Al}_2\text{O}_3$ the removal of the ARMs was slightly above 50%. The iron leaching was very low (<0.05 wt.%, regardless of the catalyst). It is worthwhile highlighting that most of the materials synthesized in this work have displayed suitable activities towards the degradation of QN, indicating the feasibility of using polymers as feedstock for producing active CNTs. Not one sample can be immediately emphasized as the best-performing one. Nevertheless, CNT-MIX-800 can be highlighted as a promising sample due to its precursor (a mixture of polyolefins, more closely resembling real PSW) and good performance.

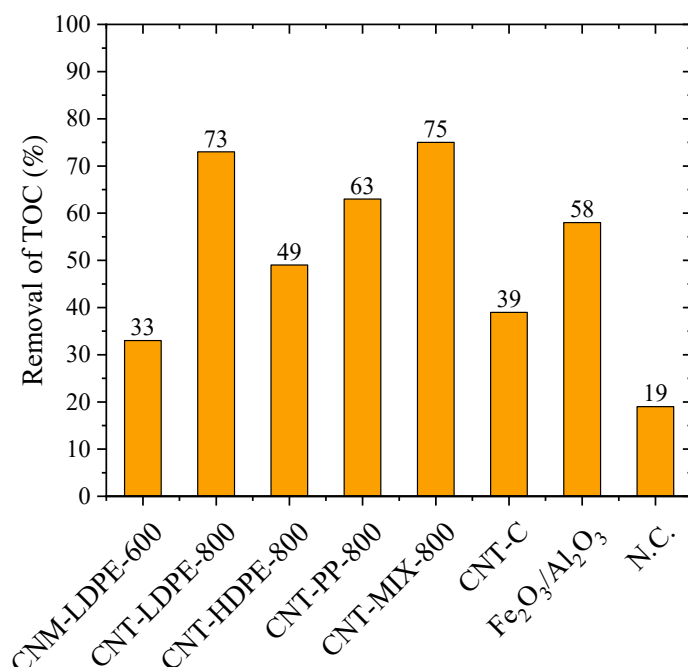


Figure 6. Removal of TOC after 24 h of reaction in the presence of the catalysts. Conditions: $\text{pH}_0 = 3.0$, $[\text{QN}]_0 = 100 \text{ mg L}^{-1}$, $c_{\text{cat}} = 2.5 \text{ g L}^{-1}$, $T = 80^\circ\text{C}$, and $[\text{H}_2\text{O}_2]_0 = 6.2 \text{ g L}^{-1}$.

The results reported here for QN degradation in an aqueous medium are similar to those reported in the literature for catalytic ozonation [59,62,63], photolysis [5], and Fenton-like systems [64].

3. Materials and Methods

3.1. Reagents and Materials

Alumina was obtained from BASF in the form of pellets. Before being used, it was ground and sieved in the 53–106 μm range. Ethanol absolute (99.8%), ethylene glycol (99%), acetonitrile (99.9%), and orthophosphoric acid (85%) were provided by Fisher Chemical (Waltham, MA, USA). Iron(II) chloride tetrahydrate (98%) was provided by Acros Organics (Geel, Belgium). Iron(III) chloride hexahydrate (98%), hydrogen peroxide (30%), and sodium hydroxide (99.2%) were obtained from VWR Chemicals (Radnor, PA, USA). High-density polyethylene (HDPE, melt index 2.2 g/10 min), low-density polyethylene (LDPE, weight average molecular weight $\sim 35,000 \text{ g mol}^{-1}$, number average molecular weight ~ 7700), polypropylene (PP, weight average molecular weight $\sim 250,000 \text{ g mol}^{-1}$, number av-

erage molecular weight ~67,000), titanium(IV) oxysulfate (~15 wt.% in diluted sulfuric acid, 99.99% trace metal basis), and multi-walled carbon nanotubes (O.D. \times L 6–9 nm \times 5 μ m, >95% carbon) were obtained from Sigma-Aldrich (St. Louis, MI, USA). Quinoline (98%) and sulfuric acid (98%) were obtained from Alfa Aesar (Haverhill, MA, USA) and Labkem (Lucknow, India), respectively. All reactants were used without modifications. Ultrapure water was used throughout the work.

3.2. Synthesis of Carbon Nanotubes

The CNTs were synthesized via chemical vapor deposition (CVD) over an iron-based catalyst supported in alumina ($\text{Fe}_2\text{O}_3/\text{Al}_2\text{O}_3$) following a sol-gel methodology, as previously described [65]. The sol-gel procedure was conducted as follows: 10 mmol of FeCl_2 was dissolved in 20 mL of ethanol and heated until reaching its boiling point, and 20 mmol of FeCl_3 was dissolved in 80 mL of ethylene glycol and heated to 60 °C for 5 min. Both solutions were then inserted into an ice bath until reaching temperature equilibrium. The choice of a $\text{M}^{+2}/\text{M}^{+3}$ molar ratio of 2 was based on previous works related to the sol-gel synthesis of other ferrites [66,67]. The solutions were mixed in one beaker with Al_2O_3 (6.6 g), and the mixture was heated to 60 °C for 2 h in a heating plate with stirring. Then, the temperature was increased to 120 °C, and the mixture was left at this temperature until reaching a gel-like texture (*ca.* 3 h). Once the gel-like texture was achieved, the temperature was increased to 200 °C until a powder texture was reached. The obtained powder was subjected to thermal treatment under nitrogen flow (100 mL min^{-1}) at 300 °C for 12 h and 600 °C for 24 h, leading to $\text{Fe}_2\text{O}_3/\text{Al}_2\text{O}_3$.

The CVD process occurred in a vertical oven (TH/TV, Termolab), considering LDPE, HDPE, PP, and a mixture of the three polymers (MIX) as carbon sources. The mixture of three polymers consisted of 35:25:40 of LDPE: HDPE: PP (in mass basis). The proportion was chosen based on a commonly found composition for waste municipal streams [18]. The oven has an upper and a lower crucible and three regions of temperature control (T_1 , T_2 , and T_3), as shown elsewhere [12]. For the growth of CNMs, 1 g of the catalyst $\text{Fe}_2\text{O}_3/\text{Al}_2\text{O}_3$ was loaded in the lower crucible and 5 g of the desired polymer (or a mixture of polymers) on the upper crucible, as previously described [19]. The synthesis was conducted at $T_3 = 800$ °C with a 1 h hold time upon reaching the desired temperature under the nitrogen flow (40 mL min^{-1}). One sample derived from LDPE was also synthesized at $T_3 = 600$ °C and 40 mL min^{-1} of nitrogen flow. The yield of CNMs was calculated according to Equation (1):

$$\text{Yield}(\%) = \frac{m_{\text{recovered}} * \%C_{\text{material}}}{m_{\text{polyolefin}} * \%C_{\text{polymer}}} \quad (1)$$

where $m_{\text{recovered}}$ is the mass of the sample recovered by the end of the CVD process (in g), $\%C_{\text{material}}$ is the percentual of elemental carbon in the material obtained after CVD as determined by elemental analysis (in wt.%), $m_{\text{polyolefin}}$ is the mass of the polymer used for the CVD process (in g), and $\%C_{\text{polymer}}$ is the content of carbon in the polymeric materials (85.6 wt.%). A blank experiment was performed consisting of an equal thermal treatment of the catalyst (without further feedstock) in order to know whether the catalyst showed significant mass changes, i.e., affected the yield calculation.

After synthesis, the CNTs were subjected to acid washing (purification) to reduce the quantity of $\text{Fe}_2\text{O}_3/\text{Al}_2\text{O}_3$ attached to the structure (50% *v/v* H_2SO_4 , 140 °C, 3 h, under reflux), as described elsewhere [13]. After it were cooled down, the material was abundantly washed with distilled water to remove excess acid and dried at 60 °C for over 12 h. The samples were labeled according to the polymeric feedstock and temperature as follows: CNM-LDPE-600 (as it did not result in a CNT), CNT-LDPE-800, CNT-HDPE-800, CNT-PP-800, and CNT-MIX-800. The mass loss of purified CNTs was calculated according to Equation (2):

$$\text{Mass loss}(\%) = \left(1 - \frac{m_{\text{CNT,P}}}{m_{\text{CNT,O}}} \right) \times 100 \quad (2)$$

where $m_{\text{CNT,P}}$ is the mass of CNT recovered after washing (in g) and $m_{\text{CNT,O}}$ is the mass of CNT used for the washing process (in g).

3.3. Materials Characterization

X-ray diffraction (XRD) analyses were made, at room temperature, with a PANalytical X' Pert Pro diffractometer equipped with an X' Celerator detector and secondary monochromator in $\theta/2\theta$ Bragg-Brentano geometry. The measurements were carried out using 40 kV and 30 mA, a CuK α radiation ($\lambda\alpha_1 = 1.54060 \text{ \AA}$ and $\lambda\alpha_2 = 1.54443 \text{ \AA}$), $0.017^\circ/\text{step}$, and 100 s/step , in a $10\text{--}80^\circ 2\theta$ angular range. The FT-IR spectrum was acquired using a Perkin Elmer FTIR-UATR with a resolution of 4 cm^{-1} from 400 to 4000 cm^{-1} , using the KBr pellet method. TEM images were obtained using a JEOL 1011 transmission electron microscope operating at 200 kV. Thermogravimetric analysis (TGA) was conducted using a NETZSCH TG 209F3 in an air atmosphere from 30 to 930°C at a rate of $10^\circ\text{C min}^{-1}$. The remaining weight of the samples after TG analysis was used to determine the ash content. Textural properties of the materials were determined from N_2 adsorption/desorption isotherms at -196°C obtained in a Quantachrome instrument NOVA TOUCH LX4 (Quantachrome Instruments, Florida, USA) as described elsewhere [13]. The Fe content of the CNTs was determined by digesting the ashes of the CNTs with aqua regia (HNO_3 : $\text{HCl} = 1:3$, molar ratio) at 105°C for 12 h. The resulting liquid was filtered with a $0.45 \mu\text{m}$ syringe filter and analyzed via atomic absorption spectroscopy (PinAacle 900 T, Perkin Elmer, Hongkong, China). The elemental analysis (CHNS-O) was carried out in a Flash 2000 analyzer (Thermo Fisher Scientific, Waltham, MA, USA) provided with a thermal conductivity detector (TCD).

3.4. Reaction Runs

3.4.1. Catalytic Wet Peroxide Oxidation (CWPO) of QN

A QN solution ($[\text{QN}]_0 = 100 \text{ mg L}^{-1}$) in ultrapure water set at pH 3.0 (not buffered) was placed in a reaction vessel and heated to the desired temperature (80°C). Upon reaching the temperature, hydrogen peroxide was added ($[\text{H}_2\text{O}_2]_0 = 6.2 \text{ g L}^{-1}$). Then, the catalyst ($c_{\text{catalyst}} = 2.5 \text{ g L}^{-1}$) was added, considering this as $t_0 = 0 \text{ min}$. QN and H_2O_2 concentrations along the reaction were monitored via HPLC and UV-Vis, respectively. Upon withdrawing the reaction samples, they were immediately submerged in an ice bath and kept at 4°C for subsequent analysis. By the end of the reaction, the catalyst was separated from the reaction, and the resulting liquid was analyzed by TOC, pH, and other aromatic compounds (ARMs). A non-catalytic (N.C.) run was carried out under the same conditions without the catalyst.

3.4.2. Analytical Techniques

The H_2O_2 concentration was determined using a TiOSO_4 methodology and measured using UV-Vis (UV-VIS Spectrometer, T70, PG Instrument Ltd., Lutterworth, UK) at 405 nm , as described elsewhere [14]. The QN concentration in the water phase was followed via high-performance liquid chromatography (HPLC). The separation of QN and reaction products was achieved using a JASCO HPLC system coupled to a Nucleosil 100-5C18 ($150 \times 2.1 \text{ mm}$) column. A mobile phase consisting of 20% of acetonitrile and 80% of a phosphate buffer solution (17 mmol) at pH 6.5 (isocratic) was delivered at a 0.5 mL min^{-1} flow rate by a quaternary gradient pump (PU-2089). Detection was achieved in a UV-Vis detector (UV-2075) at 313 nm . The TOC was measured in TOC-L (Shimadzu, Kyoto, Japan) equipment. Aromatic compounds (ARMs) were estimated by diluting the samples with a phosphate buffer solution at a pH of 7.0 and analyzed via UV-Vis at 254 nm [12].

4. Conclusions

Graphitic carbon samples were successfully synthesized from representative fractions of PSW at 600 and 800°C . All samples synthesized at 800°C have resulted in the desired carbon nanotube structure. In all cases, higher amounts of ashes were observed compared to a commercial sample. However, the synthesis conducted at 600°C resulted in a graphitic shell around the catalyst particles rather than carbon nanotubes. Nonetheless, the present study

demonstrates that CNTs can be synthesized in a one-stage reactor from simulated PSW with interesting yields when the temperature is correctly selected. Further investigations into using real plastic waste are still needed to fully evaluate the proposed solution.

All samples were active in the abatement of QN via CWPO, resulting in complete QN degradation in 30 min under the best scenario and 120 min under the worst scenario. Up to 75% of mineralization was observed, with the remaining TOC content being likely ascribed to the formation of low-molecular-weight carboxylic acids, corroborated by the reduction in the pH of the effluent and the high removals of other aromatic compounds. Thus, CNTs derived from plastic waste could be useful catalysts for wastewater treatment. As far as we are aware, no other works report the use of waste-derived CNT samples for QN degradation.

Supplementary Materials: The following supporting information can be downloaded at: <https://www.mdpi.com/article/10.3390/catal13091259/s1>. It includes the COD reference cards for XRD analysis (Figure S1), TEM images of CNM-LDPE-600 (Figure S2), the yield of the carbon samples after CVD (Figure S3), the N₂ adsorption-desorption isotherms (Figure S4), Intermediates compounds in N.C. run, final pH of the reactions and ARM abatement (Figure S5).

Author Contributions: Conceptualization: F.F.R. and J.L.D.d.T.; methodology: F.F.R., L.D.G.P. and J.L.D.d.T.; formal analysis: F.F.R. and L.D.G.P.; investigation: F.F.R., L.D.G.P. and I.V.K.F.; data curation: F.F.R. and A.S.S.; visualization: F.F.R. and A.S.S.; writing—original draft preparation: F.F.R. and A.S.S.; writing—review and editing: J.L.D.d.T., A.V., G.G.L., A.M.T.S., J.L.F. and H.T.G.; supervision: A.M.T.S., J.L.F. and H.T.G.; project administration: J.L.D.d.T. and H.T.G.; funding acquisition: J.L.D.d.T. and H.T.G. All authors have read and agreed to the published version of the manuscript.

Funding: This work was financially supported by LA/P/0045/2020 (ALiCE), UIDB/50020/2020 and UIDP/50020/2020 (LSRE-LCM) funded by national funds through FCT/MCTES (PIDDAC), and CIMO (UIDB/00690/2020) through FEDER under Program PT2020, project “PLASTIC_TO_FUEL&MAT—Upcycling Waste Plastics into Fuel and Carbon Nanomaterials” (PTDC/EQU-EQU/31439/2017). Fernanda F. Roman acknowledges the national funding from the FCT and the European Social Fund, FSE, through the individual research grant SFRH/BD/143224/2019. Adriano Santos Silva thanks the FCT for financial support under the MIT Portugal Program with doctoral grant SFRH/BD/151346/2021. J. L. Diaz de Tuesta acknowledges the research grants (2022-T1/AMB-23946) from the program of Atracción al Talento of Comunidad de Madrid (Spain).

Data Availability Statement: Data will be available upon request.

Conflicts of Interest: The authors declare no conflict of interest.

References

1. Huang, L.; Liu, Z.; Dong, H.; Yu, T.; Jiang, H.; Peng, Y.; Shi, L. Coupling quinoline degradation with Fe redox in clay minerals: A strategy integrating biological and physicochemical processes. *Appl. Clay Sci.* **2020**, *188*, 105504. [CrossRef]
2. Saber, A.N.; Zhang, H.; Cervantes-Avilés, P.; Islam, A.; Gao, Y.; An, W.; Yang, M. Emerging concerns of VOCs and SVOCs in coking wastewater treatment processes: Distribution profile, emission characteristics, and health risk assessment. *Environ. Pollut.* **2020**, *265*, 114960. [CrossRef] [PubMed]
3. Kang, W.; Cui, Y.; Yang, Y.; Zhao, Z.; Wang, X.; Liu, X. An acid induction strategy to construct an ultralight and durable amino-functionalized graphene oxide aerogel for enhanced quinoline pollutants extraction from coking wastewater. *Chem. Eng. J.* **2021**, *412*, 128686. [CrossRef]
4. Liu, Y.; Liu, J.; Zhang, A.; Liu, Z. Treatment effects and genotoxicity relevance of the toxic organic pollutants in semi-coking wastewater by combined treatment process. *Environ. Pollut.* **2017**, *220*, 13–19. [CrossRef] [PubMed]
5. Zhang, W.-B.; An, T.-C.; Xiao, X.-M.; Fu, J.-M.; Sheng, G.-Y.; Cui, M.-C. Photochemical degradation performance of quinoline aqueous solution in the presence of hydrogen peroxide. *J. Environ. Sci. Health Part A Toxic/Hazard. Subst. Environ. Eng.* **2003**, *38*, 2599–2611. [CrossRef] [PubMed]
6. Chen, J.; Zhang, B.; Wang, B.; Cui, C.; Wang, S.; Wang, J.; Zhang, W. Enhanced degradation of quinoline in three-dimensional electro-Fenton system using catalytic Fe-Co-Ni-P/g-C₃N₄ particles. *Int. J. Electrochem. Sci.* **2022**, *17*, 221296. [CrossRef]
7. Zhang, B.; You, H.; Wang, F. Microwave-enhanced catalytic wet peroxide oxidation of quinoline: The influence of pH and H₂O₂ dosage and identification of reactive oxygen species. *RSC Adv.* **2017**, *7*, 14769–14775. [CrossRef]

8. Wang, S.; Zhou, L.; Zheng, M.; Han, J.; Liu, R.; Yun, J. Catalytic Ozonation over $\text{Ca}_2\text{Fe}_2\text{O}_5$ for the Degradation of Quinoline in an Aqueous Solution. *Ind. Eng. Chem. Res.* **2022**. *epub ahead of print*. [CrossRef]
9. Zhang, L.; Fan, L.; Fan, J.; Li, Y.; Sun, P.; Han, J.; Fan, Z. Synergistic effects of $\text{Vis}/\text{H}_2\text{O}_2/\text{LaFe}_{1-x}\text{Cu}_x\text{O}_3$ and $\text{Vis}/\text{PDS}/\text{LaFe}_{1-x}\text{Cu}_x\text{O}_3$ for quinoline degradation: Performance and mechanism. *J. Environ. Chem. Eng.* **2022**, *10*, 108322. [CrossRef]
10. Diaz de Tuesta, J.L.; Quintanilla, A.; Casas, J.A.; Morales-Torres, S.; Faria, J.L.; Silva, A.M.T.; Gomes, H.T. The pH effect on the kinetics of 4-nitrophenol removal by CWPO with doped carbon black catalysts. *Catal. Today* **2020**, *356*, 216–225. [CrossRef]
11. Diaz de Tuesta, J.L.; Quintanilla, A.; Moreno, D.; Ferro, V.R.; Casas, J.A. Simulation and optimization of the CWPO process by combination of aspen plus and 6-factor doehlert matrix: Towards autothermal operation. *Catalysts* **2020**, *10*, 548. [CrossRef]
12. Diaz de Tuesta, J.L.; Silva, A.S.; Roman, F.F.; Sanches, L.F.; da Silva, F.A.; Pereira, A.I.; Silva, A.M.T.; Faria, J.L.; Gomes, H.T. Polyolefin-derived carbon nanotubes as magnetic catalysts for wet peroxide oxidation of paracetamol in aqueous solutions. *Catal. Today* **2023**, *419*, 114162. [CrossRef]
13. Roman, F.F.; Diaz de Tuesta, J.L.; Sanches, F.K.K.; Silva, A.S.; Marin, P.; Machado, B.F.; Serp, P.; Pedrosa, M.; Silva, A.M.T.; Faria, J.L.; et al. Selective denitrification of simulated oily wastewater by oxidation using Janus-structured carbon nanotubes. *Catal. Today* **2023**, *420*, 114001. [CrossRef]
14. Silva, A.S.; Kalmakhanova, M.S.; Massalimova, B.K.; de Tuesta, J.L.D.; Gomes, H.T. Wet peroxide oxidation of paracetamol using acid activated and Fe/Co-pillared clay catalysts prepared from natural clays. *Catalysts* **2019**, *9*, 705. [CrossRef]
15. Guari, N.M.C.; Silva, A.S.; Diaz de Tuesta, J.L.; Pottker, W.E.; Cordeiro, P.Y.; Gomes, H.T. Magnetic CoFe_2O_4 @carbon yolk-shell nanoparticles as catalysts for the catalytic wet peroxide oxidation of paracetamol: Kinetic insights. *Glob. NEST J.* **2022**, *25*, 57–66. [CrossRef]
16. De Freitas Batista, G.; Roman, F.F.; de Tuesta, J.L.D.; Mambrini, R.V.; Praça, P.; Gomes, H.T. Assessment of Pretreatments for Highly Concentrated Leachate Waters to Enhance the Performance of Catalytic Wet Peroxide Oxidation with Sustainable Low-Cost Catalysts. *Catalysts* **2022**, *12*, 238. [CrossRef]
17. Lau, W.W.Y.; Shiran, Y.; Bailey, R.M.; Cook, E.; Stuchtey, M.R.; Koskella, J.; Velis, C.A.; Godfrey, L.; Boucher, J.; Murphy, M.B.; et al. Evaluating scenarios toward zero plastic pollution. *Science* **2020**, *369*, 1455–1461. [CrossRef]
18. PlasticsEurope. Plastics—the Facts 2022. Available online: <https://plasticseurope.org/knowledge-hub/plastics-the-facts-2022/> (accessed on 10 July 2023).
19. Ribeiro, R.S.; Vieira, O.; Fernandes, R.; Roman, F.F.; Diaz de Tuesta, J.L.; Silva, A.M.T.T.; Gomes, H.T. Synthesis of low-density polyethylene derived carbon nanotubes for activation of persulfate and degradation of water organic micropollutants in continuous mode. *J. Environ. Manag.* **2022**, *308*, 114622. [CrossRef]
20. Vieira, O.; Ribeiro, R.S.; Diaz de Tuesta, J.L.; Gomes, H.T.; Silva, A.M.T. A systematic literature review on the conversion of plastic wastes into valuable 2D graphene-based materials. *Chem. Eng. J.* **2022**, *428*, 131399. [CrossRef]
21. Cai, N.; Li, X.; Xia, S.; Sun, L.; Hu, J.; Bartocci, P.; Fantozzi, F.; Williams, P.T.; Yang, H.; Chen, H. Pyrolysis-catalysis of different waste plastics over Fe/ Al_2O_3 catalyst: High-value hydrogen, liquid fuels, carbon nanotubes and possible reaction mechanisms. *Energy Convers. Manag.* **2021**, *229*, 113794. [CrossRef]
22. Mukherjee, A.; Debnath, B.; Ghosh, S.K. *Carbon Nanotubes as a Resourceful Product Derived from Waste Plastic—A Review BT-Waste Management and Resource Efficiency*; Ghosh, S.K., Ed.; Springer: Singapore, 2019; pp. 915–934.
23. Aboul-Enein, A.A.; Awadallah, A.E.; Abdel-Rahman, A.A.H.; Haggag, A.M. Synthesis of multi-walled carbon nanotubes via pyrolysis of plastic waste using a two-stage process. *Fullerenes Nanotub. Carbon Nanostruct.* **2018**, *26*, 443–450. [CrossRef]
24. Yang, R.X.; Chuang, K.H.; Wey, M.Y. Effects of Temperature and Equivalence Ratio on Carbon Nanotubes and Hydrogen Production from Waste Plastic Gasification in Fluidized Bed. *Energy Fuels* **2018**, *32*, 5462–5470. [CrossRef]
25. Liu, X.; Shen, B.; Wu, Z.; Parlett, C.M.A.; Han, Z.; George, A.; Yuan, P.; Patel, D.; Wu, C. Producing carbon nanotubes from thermochemical conversion of waste plastics using Ni/ceramic based catalyst. *Chem. Eng. Sci.* **2018**, *192*, 882–891. [CrossRef]
26. Wyss, K.M.; De Kleine, R.D.; Couvreur, R.L.; Kiziltas, A.; Mielewski, D.F.; Tour, J.M. Upcycling end-of-life vehicle waste plastic into flash graphene. *Commun. Eng.* **2022**, *1*, 3. [CrossRef]
27. Dai, L.; Karakas, O.; Cheng, Y.; Cobb, K.; Chen, P.; Ruan, R. A review on carbon materials production from plastic wastes. *Chem. Eng. J.* **2023**, *453*, 139725. [CrossRef]
28. Zhuo, C.; Levendis, Y.A. Upcycling waste plastics into carbon nanomaterials: A review. *J. Appl. Polym. Sci.* **2014**, *131*, 1–14. [CrossRef]
29. Kumar, R.; Singh, R.K.; Singh, D.P. Natural and waste hydrocarbon precursors for the synthesis of carbon based nanomaterials: Graphene and CNTs. *Renew. Sustain. Energy Rev.* **2016**, *58*, 976–1006. [CrossRef]
30. Hazan, M.A.; Chan, K.F.; Jofri, K.A.; Mamat, M.S.; Endot, N.A.; Liza, S.; Ismail, I.; Hussein, M.Z.; Tanemura, M.; Yaakob, Y. Waste nr latex based-precursors as carbon source for cnts eco-fabrications. *Polymers* **2021**, *13*, 3409. [CrossRef]
31. Dai, L.; Zhou, N.; Lv, Y.; Cheng, Y.; Wang, Y.; Liu, Y.; Cobb, K.; Chen, P.; Lei, H.; Ruan, R. Pyrolysis technology for plastic waste recycling: A state-of-the-art review. *Prog. Energy Combust. Sci.* **2022**, *93*, 101021. [CrossRef]
32. Wang, X.; Zhao, Z.; Qu, J.; Wang, Z.; Qiu, J. Fabrication and characterization of magnetic Fe_3O_4 -CNT composites. *J. Phys. Chem. Solids* **2010**, *71*, 673–676. [CrossRef]
33. Kazemifard, S.; Nayebezhadeh, H.; Saghatoleslami, N.; Safakish, E. Assessment the activity of magnetic $\text{KOH}/\text{Fe}_3\text{O}_4/\text{Al}_2\text{O}_3$ core-shell nanocatalyst in transesterification reaction: Effect of Fe/Al ratio on structural and performance. *Environ. Sci. Pollut. Res.* **2018**, *25*, 32811–32821. [CrossRef] [PubMed]

34. Harutyunyan, A.R.; Pradhan, B.K.; Kim, U.J.; Chen, G.; Eklund, P.C. CVD Synthesis of Single Wall Carbon Nanotubes under “Soft” Conditions. *Nano Lett.* **2002**, *2*, 525–530. [\[CrossRef\]](#)
35. Gakis, G.P.; Termine, S.; Trompeta, A.F.A.; Aviziotis, I.G.; Charitidis, C.A. Unraveling the mechanisms of carbon nanotube growth by chemical vapor deposition. *Chem. Eng. J.* **2022**, *445*, 136807. [\[CrossRef\]](#)
36. Lee, C.J.; Park, J.; Yu, J.A. Catalyst effect on carbon nanotubes synthesized by thermal chemical vapor deposition. *Chem. Phys. Lett.* **2002**, *360*, 250–255. [\[CrossRef\]](#)
37. Veksha, A.; Chen, W.; Liang, L.; Lisak, G. Converting polyolefin plastics into few-walled carbon nanotubes via a tandem catalytic process: Importance of gas composition and system configuration. *J. Hazard. Mater.* **2022**, *435*, 128949. [\[CrossRef\]](#) [\[PubMed\]](#)
38. Cui, J.; Tan, S.; Song, R. Universal Ni-Mo-Mg catalysts combined with carbon blacks for the preparation of carbon nanotubes from polyolefins. *J. Appl. Polym. Sci.* **2017**, *134*. [\[CrossRef\]](#)
39. Pinho, M.T.; Gomes, H.T.; Ribeiro, R.S.; Faria, J.L.; Silva, A.M.T. Carbon nanotubes as catalysts for catalytic wet peroxide oxidation of highly concentrated phenol solutions: Towards process intensification. *Appl. Catal. B Environ.* **2015**, *165*, 706–714. [\[CrossRef\]](#)
40. Raji, K.; Thomas, S.; Sobhan, C.B. A chemical kinetic model for chemical vapor deposition of carbon nanotubes. *Appl. Surf. Sci.* **2011**, *257*, 10562–10570. [\[CrossRef\]](#)
41. Toussi, S.M.; Fakhru’L-Razi, A.; Chuah, A.L.; Suraya, A.R. Effect of synthesis condition on the growth of SWCNTs via catalytic chemical vapour deposition. *Sains Malays.* **2011**, *40*, 197–201.
42. Niu, Z.; Fang, Y. Effect of temperature for synthesizing single-walled carbon nanotubes by catalytic chemical vapor deposition over Mo-Co-MgO catalyst. *Mater. Res. Bull.* **2008**, *43*, 1393–1400. [\[CrossRef\]](#)
43. Williams, P.T. Hydrogen and Carbon Nanotubes from Pyrolysis-Catalysis of Waste Plastics: A Review. *Waste Biomass Valorization* **2021**, *12*, 1–28. [\[CrossRef\]](#)
44. Aguado, J.; Serrano, D.P.; Escola, J.M.; Garagorri, E.; Fernández, J.A. Catalytic conversion of polyolefins into fuels over zeolite beta. *Polym. Degrad. Stab.* **2000**, *69*, 11–16. [\[CrossRef\]](#)
45. Zhou, Q.; Zheng, L.; Wang, Y.Z.; Zhao, G.M.; Wang, B. Catalytic degradation of low-density polyethylene and polypropylene using modified ZSM-5 zeolites. *Polym. Degrad. Stab.* **2004**, *84*, 493–497. [\[CrossRef\]](#)
46. Yan, G.; Jing, X.; Wen, H.; Xiang, S. Thermal cracking of virgin and waste plastics of PP and LDPE in a semibatch reactor under atmospheric pressure. *Energy Fuels* **2015**, *29*, 2289–2298. [\[CrossRef\]](#)
47. Sengupta, J.; Jacob, C. Growth temperature dependence of partially Fe filled MWCNT using chemical vapor deposition. *J. Cryst. Growth* **2009**, *311*, 4692–4697. [\[CrossRef\]](#)
48. Țucureanu, V.; Matei, A.; Avram, A.M. FTIR Spectroscopy for Carbon Family Study. *Crit. Rev. Anal. Chem.* **2016**, *46*, 502–520. [\[CrossRef\]](#) [\[PubMed\]](#)
49. Scheibe, B.; Borowiak-Palen, E.; Kalenczuk, R.J. Oxidation and reduction of multiwalled carbon nanotubes-preparation and characterization. *Mater. Charact.* **2010**, *61*, 185–191. [\[CrossRef\]](#)
50. Zhong, B.; Huang, R.; Su, D.S.; Liu, H. Effect of graphitization of oxygen-modified carbon nanotubes in selective oxidation of acrolein. *Catal. Today* **2019**, *330*, 142–148. [\[CrossRef\]](#)
51. Likodimos, V.; Steriotis, T.A.; Papageorgiou, S.K.; Romanos, G.E.; Marques, R.R.N.; Rocha, R.P.; Faria, J.L.; Pereira, M.F.R.; Figueiredo, J.L.; Silva, A.M.T.; et al. Controlled surface functionalization of multiwall carbon nanotubes by HNO₃ hydrothermal oxidation. *Carbon* **2014**, *69*, 311–326. [\[CrossRef\]](#)
52. Oliveira, A.A.S.; Teixeira, I.F.; Christofani, T.; Tristão, J.C.; Guimarães, I.R.; Moura, F.C.C. Biphasic oxidation reactions promoted by amphiphilic catalysts based on red mud residue. *Appl. Catal. B Environ.* **2014**, *144*, 144–151. [\[CrossRef\]](#)
53. Zhang, Q.; Sun, Y.; Han, Y.; Li, Y.; Gao, P. Review on coal-based reduction and magnetic separation for refractory iron-bearing resources. *Int. J. Miner. Metall. Mater.* **2022**, *29*, 2087–2105. [\[CrossRef\]](#)
54. Leventis, N.; Donthula, S.; Mandal, C.; Ding, M.S.; Sotiriou-Leventis, C. Explosive versus Thermite Behavior in Iron(0) Aerogels Infiltrated with Perchlorates. *Chem. Mater.* **2015**, *27*, 8126–8137. [\[CrossRef\]](#)
55. Greenlee, L.F.; Hooker, S.A. Development of stabilized zero valent iron nanoparticles. *Desalin. Water Treat.* **2012**, *37*, 114–121. [\[CrossRef\]](#)
56. Ribeiro, R.S.; Frontistis, Z.; Mantzavinos, D.; Venieri, D.; Antonopoulou, M.; Konstantinou, I.; Silva, A.M.T.; Faria, J.L.; Gomes, H.T. Magnetic carbon xerogels for the catalytic wet peroxide oxidation of sulfamethoxazole in environmentally relevant water matrices. *Appl. Catal. B Environ.* **2016**, *199*, 170–186. [\[CrossRef\]](#)
57. Zhu, R.; Zhu, Y.; Xian, H.; Yan, L.; Fu, H.; Zhu, G.; Xi, Y.; Zhu, J.; He, H. CNTs/ferrihydrite as a highly efficient heterogeneous Fenton catalyst for the degradation of bisphenol A: The important role of CNTs in accelerating Fe(III)/Fe(II) cycling. *Appl. Catal. B Environ.* **2020**, *270*, 118891. [\[CrossRef\]](#)
58. Ribeiro, R.S.; Silva, A.M.T.; Figueiredo, J.L.; Faria, J.L.; Gomes, H.T. Catalytic wet peroxide oxidation: A route towards the application of hybrid magnetic carbon nanocomposites for the degradation of organic pollutants. A review. *Appl. Catal. B Environ.* **2016**, *187*, 428–460. [\[CrossRef\]](#)
59. Liu, D.; Wang, C.; Song, Y.; Wei, Y.; He, L.; Lan, B.; He, X.; Wang, J. Effective mineralization of quinoline and bio-treated coking wastewater by catalytic ozonation using CuFe₂O₄/Sepiolite catalyst: Efficiency and mechanism. *Chemosphere* **2019**, *227*, 647–656. [\[CrossRef\]](#) [\[PubMed\]](#)
60. Ma, X.; Bian, L.; Ding, J.; Wu, Y.; Xia, H.; Li, J. Electrochemical oxidation of quinoline aqueous solution on α -PbO₂ anode and the evolution of phytotoxicity on duckweed. *Water Sci. Technol.* **2017**, *75*, 1820–1829. [\[CrossRef\]](#)

61. Ribeiro, R.S.; Gallo, J.; Bañobre-López, M.; Silva, A.M.T.; Faria, J.L.; Gomes, H.T. Enhanced performance of cobalt ferrite encapsulated in graphitic shell by means of AC magnetically activated catalytic wet peroxide oxidation of 4-nitrophenol. *Chem. Eng. J.* **2019**, *376*, 120012. [[CrossRef](#)]
62. Huang, X.; Wang, X. Toxicity change patterns and its mechanism during the degradation of nitrogen-heterocyclic compounds by O(3)/UV. *Chemosphere* **2007**, *69*, 747–754. [[CrossRef](#)]
63. Wei, Q.; Qiao, S.; Sun, B.; Zou, H.; Chen, J.; Shao, L. Study on the treatment of simulated coking wastewater by O₃ and O₃/Fenton processes in a rotating packed bed. *RSC Adv.* **2015**, *5*, 93386–93393. [[CrossRef](#)]
64. Chu, L.; Wang, J.; Dong, J.; Liu, H.; Sun, X. Treatment of coking wastewater by an advanced Fenton oxidation process using iron powder and hydrogen peroxide. *Chemosphere* **2012**, *86*, 409–414. [[CrossRef](#)]
65. Silva, A.S.; Diaz de Tuesta, J.L.; Sayuri Berberich, T.; Delezuk Inglez, S.; Bertão, A.R.; Çaha, I.; Deepak, F.L.; Bañobre-López, M.; Gomes, H.T. Doxorubicin delivery performance of superparamagnetic carbon multi-core shell nanoparticles: pH dependence, stability and kinetic insight. *Nanoscale* **2022**, *14*, 7220–7232. [[CrossRef](#)]
66. Giannakopoulou, T.; Kompotiatis, L.; Kontogeorgakos, A.; Kordas, G. Microwave behavior of ferrites prepared via sol-gel method. *J. Magn. Magn. Mater.* **2002**, *246*, 360–365. [[CrossRef](#)]
67. Silva, A.S.; Roman, F.F.; Dias, A.V.; Diaz de Tuesta, J.L.; Narcizo, A.; da Silva, A.P.F.; Çaha, I.; Deepak, F.L.; Bañobre-López, M.; Ferrari, A.M.C.; et al. Hybrid multi-core shell magnetic nanoparticles for wet peroxide oxidation of paracetamol: Application in synthetic and real matrices. *J. Environ. Chem. Eng.* **2023**, *11*, 110806. [[CrossRef](#)]

Disclaimer/Publisher’s Note: The statements, opinions and data contained in all publications are solely those of the individual author(s) and contributor(s) and not of MDPI and/or the editor(s). MDPI and/or the editor(s) disclaim responsibility for any injury to people or property resulting from any ideas, methods, instructions or products referred to in the content.